JCB

Beati et al., https://doi.org/10.1083/jcb.201610098

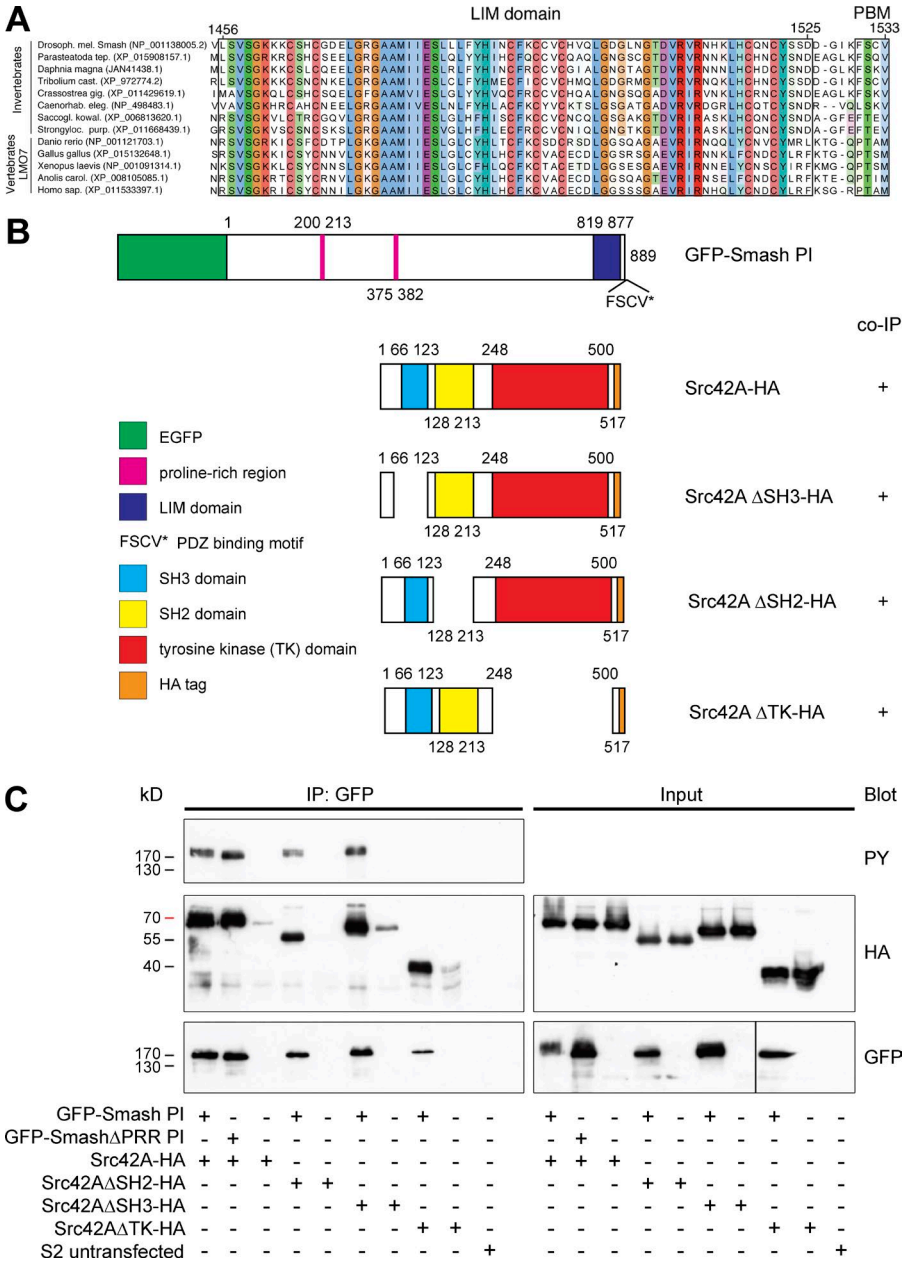


Figure S1. **The Smash PBM is conserved in evolution.** Related to Figs. 1 and 2. **(A)** Smash contains a conserved LIM-PBM module at the C terminus. Multiple sequence alignment of the C-terminal regions of Smash with its invertebrate and vertebrate LMO7 orthologues showing the conservation of the LIM-PBM module. Smash/LMO7 sequences from the indicated organisms were aligned using MUSCLE (Edgar, 2004) and color-coded in ClustalX (Chenna et al., 2003). The LIM domain and the PBM are highlighted with boxes. Database accession numbers are given in parentheses. **(B and C)** Deletion mapping of the binding interface between Smash-PI and Src42A. (B) Schematic drawings of the domain structure of GFP-Smash PI and Src42A-HA. Deletion variants of Src42A-HA used for coIP experiments are also indicated. +, coIP between GFP-Smash PI and the respective Src42A-HA version. (C) The results of coIP experiments of S2 cells doubly transfected with GFP-Smash PI constructs and Src42A-HA constructs reveal that neither mutation of the two proline-rich regions (PRR) of Smash nor deletion of either the SH2 domain, the SH3 domain, or the tyrosine kinase (TK) domain of Src42A-HA abolishes binding between GFP-Smash PI and Src42A-HA. IPs were done with anti-GFP antibodies. Antibodies used for blotting are indicated. Input controls are shown in the right panel. Note that the PY signal is absent in the lane where Src42AΔTK-HA was coimmunoprecipitated with GFP-Smash PI.

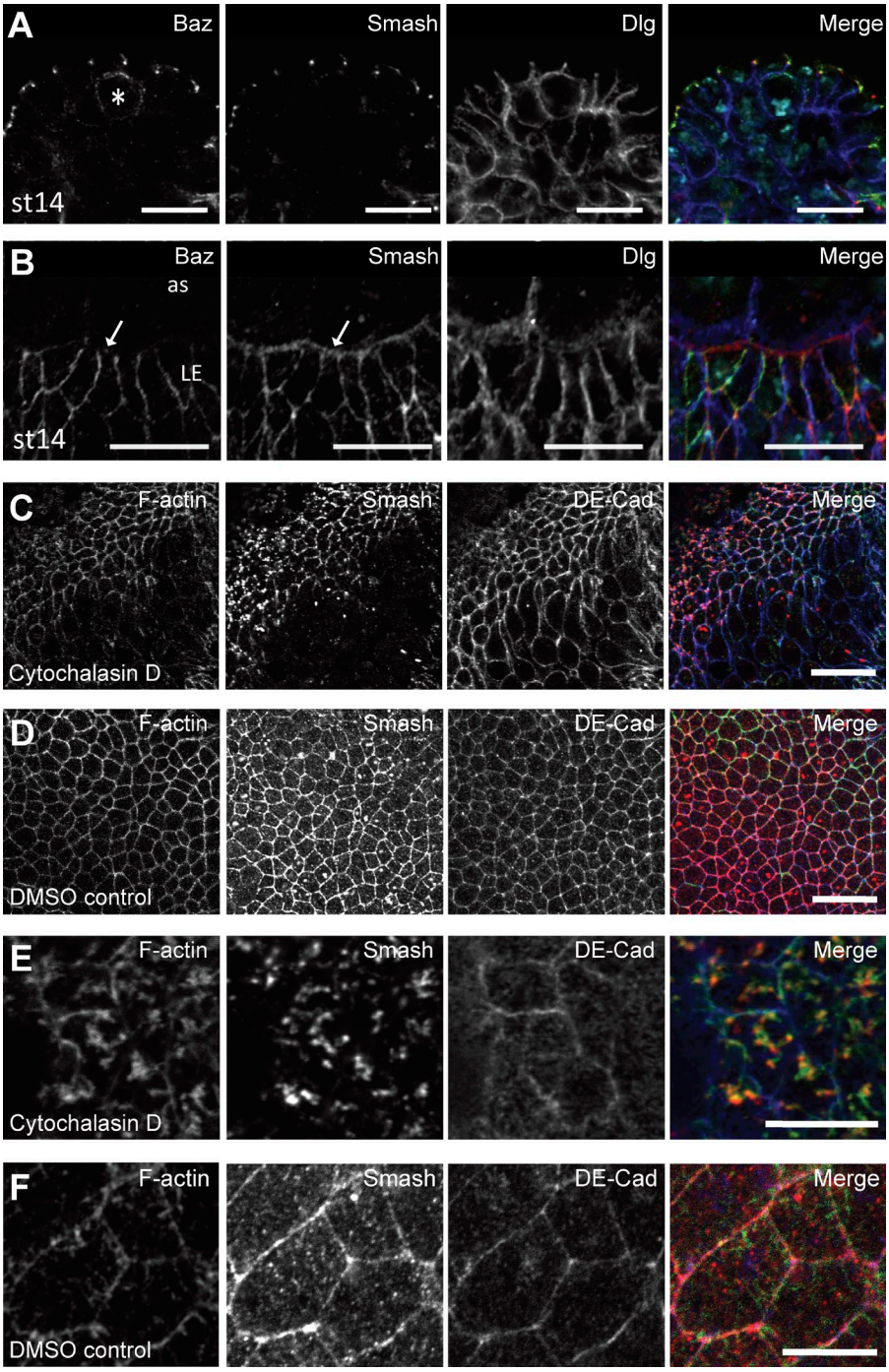


Figure S2. **Subcellular localization of Smash in embryos.** Related to Figs. 3 and 4. **(A)** A WT embryo at stage 14 was stained for Baz (A, green in Merge), Smash (red in Merge), Dlg (blue in Merge), and DNA (cyan in Merge). Note that Baz is expressed in neuroblasts (Baz, asterisk), but Smash is not (Smash). **(B)** The dorsal edge of the epidermis of a WT embryo at stage 14 was stained as in A. Note that Smash is localized at the leading edge of the dorsal most epidermal cells (Smash, arrow), whereas Baz is excluded from the leading edge (Baz, arrow). as, amnioserosa. **(C–F)** Junctional localization of Smash is dependent on F-actin. (C) Cytochalasin D treatment results in loss of F-actin and Smash from the cortex of epidermal cells of an embryo at germ band extension, whereas DE-Cad is still present. Note the nonuniform effect of cytochalasin D treatment in this embryo, which is stronger in the lower right corner of the image. (D) In DMSO-treated control embryos, F-actin colocalizes with Smash and DE-Cad at the ZA. (E) Ectopic F-actin structures induced by cytochalasin D treatment in amnioserosa cells colocalize with Smash, but not with DE-Cad. (F) Normal localization of F-actin, Smash, and DE-Cad in the amnioserosa of a DMSO-treated control embryo. In all merged images, F-actin is green, Smash is red, and DE-Cad is blue. Bars, 10 µm.

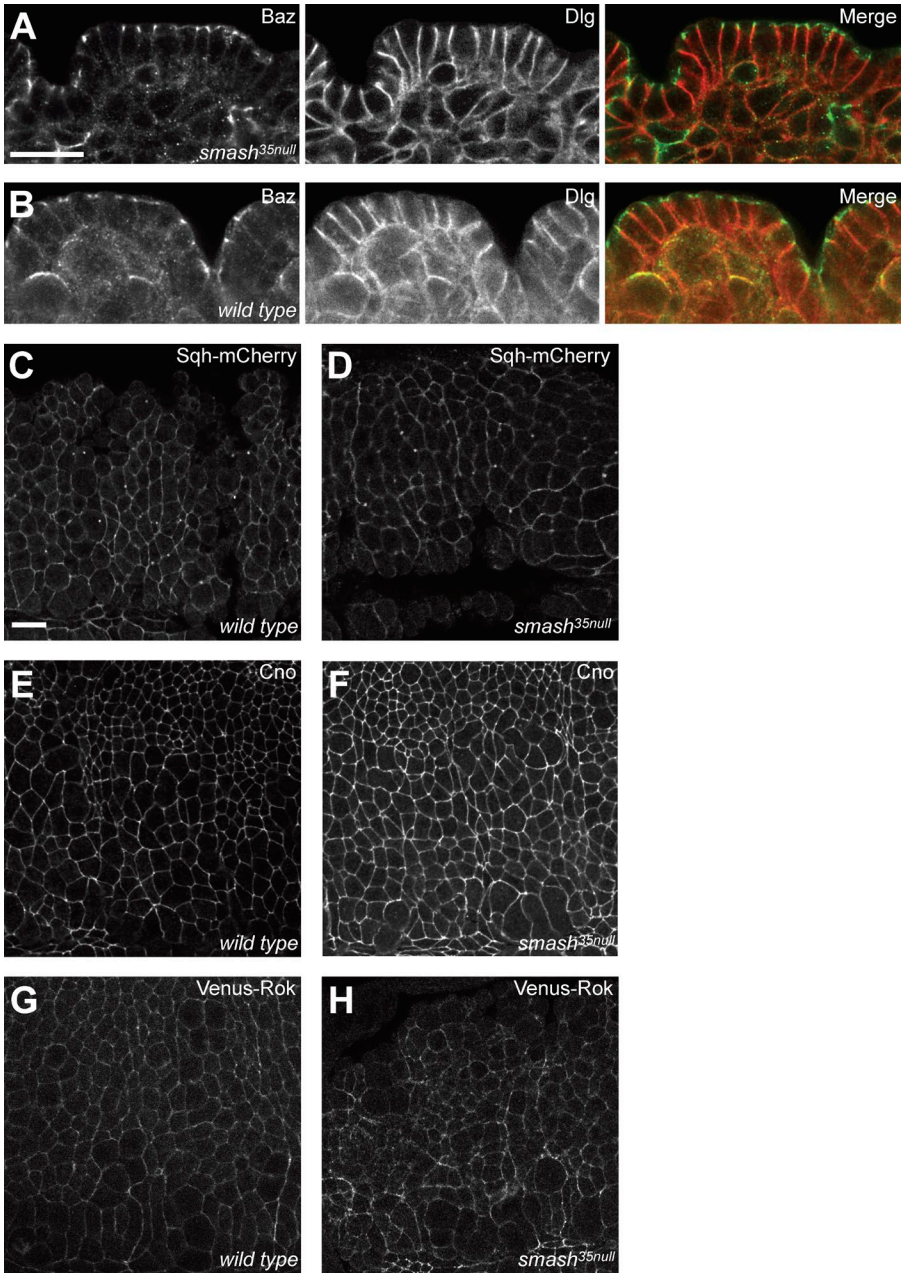


Figure S3. **Apical-basal and planar cell polarity in *smash*$^{35null}$ embryos.** Related to Figs. 4 and 7. **(A and B)** Apical-basal epithelial polarity is normal in embryos lacking maternal and zygotic Smash. A *smash*$^{35null}$ embryo (A) and a WT embryo (B) at stage 13 were stained for Baz (A and B, green in Merge) and Dlg (middle). Note that in the superficial cell layer, the neuroectodermal epithelium, the localization of Baz at the apicolateral ZA, and the localization of Dlg along the lateral plasma membrane are complementary and show little overlap. **(C–H)** Planar cell polarity of Sqh-mCherry, Cno, and Venus-Rok in WT and *smash*$^{35null}$ embryos at stage 9. In WT, Sqh-mCherry (C), Cno (E), and Venus-Rok (G) are all enriched along A/P junctions. In *smash*$^{35null}$ embryos, A/P enrichment of Sqh-mCherry (D) and Cno (F) is lost, whereas A/P enrichment of Venus-Rok (H) is unaffected. For quantification, see Fig. 5 H. Bars, 10 µm. Apical is up.

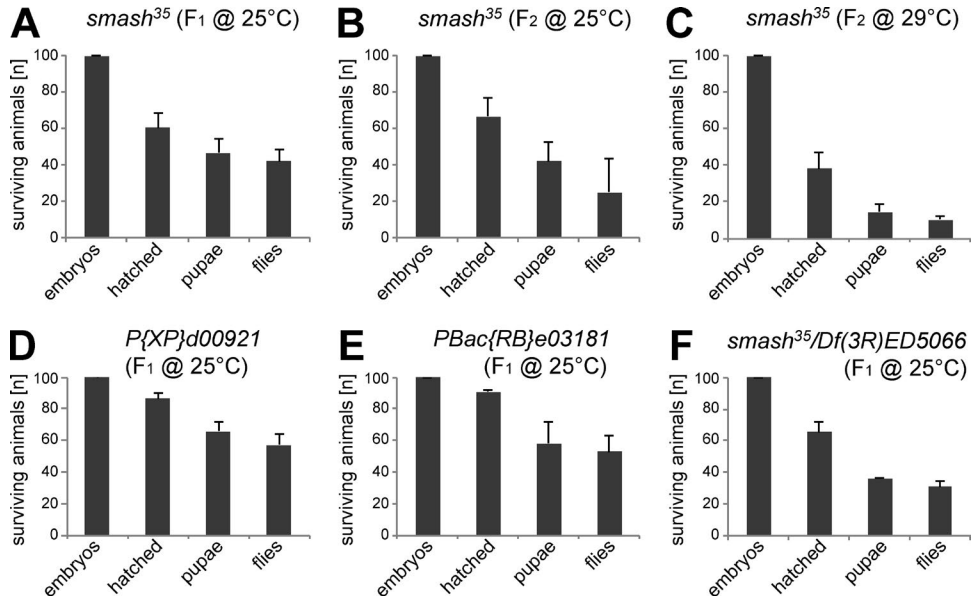


Figure S4. **Animals homozygous for *smash*$^{35}$ show reduced viability compared with animals homozygous for either of the transposon insertions used for the generation of the *smash*$^{35}$ allele.** Related to Fig. 5. **(A–C)** Survival rates of animals homozygous for *smash*$^{35}$ were analyzed at different developmental stages and temperatures. The $F_1$ animals analyzed in A were the progeny of females heterozygous for *smash*$^{35}$, whereas the $F_2$ animals analyzed in B and C were the progeny of *smash*$^{35}$ homozygous mutant females. **(D and E)** Survival rates of the two transposon insertions used for the generation of the *smash*$^{35}$ deletion. **(F)** The survival rates of animals transheterozygous for *smash*$^{35}$ and a deletion that completely removes the *smash* genomic region. Survival assays were done with $n$ = 100 embryos in triplicate. Error bars show mean + SEM.

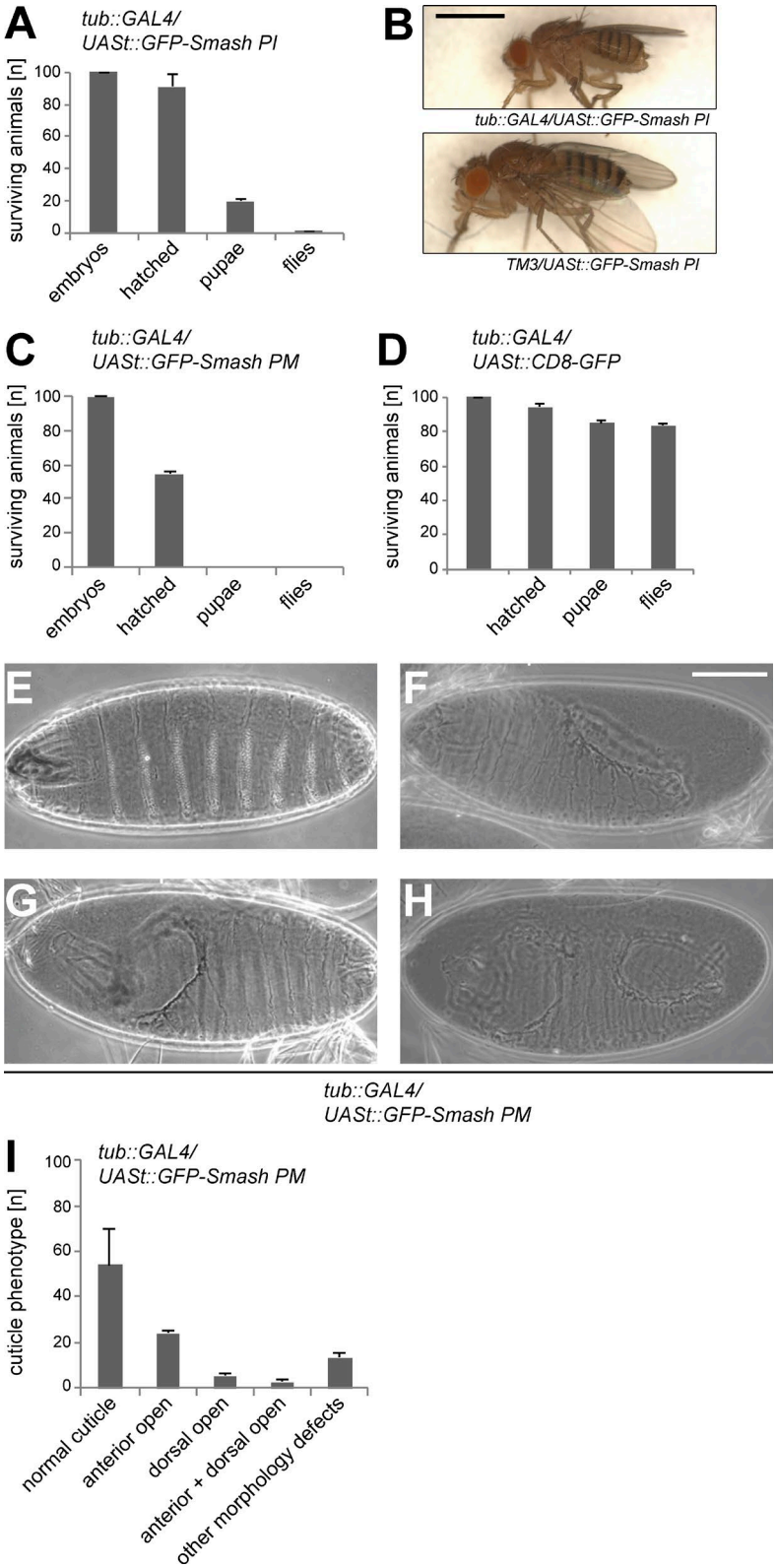


Figure S5. **Isoform-specific phenotypes of GFP-Smash overexpression.** Related to Figs. 9 and 10. **(A and B)** Quantification of survival rates of animals at different developmental stages upon ubiquitous overexpression of GFP-Smash PI. Only very few adults, which are much smaller than their control siblings lacking the GAL4 driver (B) eclose under these conditions. **(C)** Quantification of survival rates of animals at different developmental stages upon ubiquitous overexpression of GFP-Smash PM. **(D)** Quantification of survival rates of animals at different developmental stages upon ubiquitous overexpression of CD8-GFP (control). Survival assays shown in A, C, and D were done with $n$ = 100 embryos in triplicate. **(E–H)** Cuticle phenotypes of embryos overexpressing GFP-Smash PM. (E) Normal cuticle. (F) Cuticle with dorsal hole. (G) Cuticle with anterior hole. (H) Cuticle with anterior and dorsal holes. **(I)** Quantification of cuticle phenotypes of embryos overexpressing GFP-Smash PM. $n$ = 100 embryos in triplicate. Bars: (B) 1 mm; (E–H) 100 µm. Anterior is to the left. Error bars show mean + SEM.

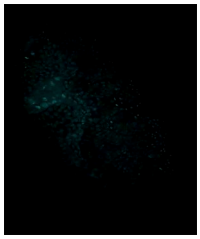

Video 1. **Abnormal morphology of a *smash*$^{35}$ null embryo at stage 7.** Corresponding to Fig. 6 (A and B). The video shows an animated z-stack of confocal images of a *smash*$^{35null}$ embryo at stage 7 stained for DAPI (cyan), Baz (red), and Dlg (blue). Each channel is first shown individually, followed by the merged channels.

Video 2. **Normal morphology of a WT embryo at stage 7.** Corresponding to Fig. 6 (C and D). The video shows an animated z-stack of confocal images of a WT embryo at stage 7 stained for DAPI (cyan), Baz (red), and Dlg (blue). Each channel is first shown individually, followed by the merged channels.

Video 3. **Abnormal morphologyof a *smash*$^{35}$ null embryo at stage 13.** Corresponding to Fig. 6 (E and F). The video shows an animated z-stack of confocal images of a *smash*$^{35null}$ embryo at stage 13 stained for DAPI (cyan), Baz (red), and Dlg (blue). Each channel is first shown individually, followed by the merged channels.

Video 4. **Normal morphology of a WT embryo at stage 13.** Corresponding to Fig. 6 (G and H). The video shows an animated z-stack of confocal images of a WT embryo at stage 13 stained for DAPI (cyan), Baz (red), and Dlg (blue). Each channel is first shown individually, followed by the merged channels.

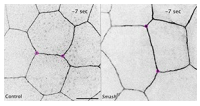

Video 5. **Laser ablation of single-cell bonds in the epidermis of *smash*$^{35null}$ and control third instar larvae.** Related to Fig. 7 (D and E). The speed and amplitude of the distance increase between vertices (magenta circles) of the ablated cell bond before and after laser ablation correlates with cell bond tension. The ZA was marked with DE-cad-GFP (black). Bar, 20 µm.

## References


Chenna, R., H. Sugawara, T. Koike, R. Lopez, T.J. Gibson, D.G. Higgins, and J.D. Thompson. 2003. Multiple sequence alignment with the Clustal series of programs. *Nucleic Acids Res.* 31:3497–3500. https://doi.org/10.1093/nar/gkg500

Edgar, R.C. 2004. MUSCLE: Multiple sequence alignment with high accuracy and high throughput. *Nucleic Acids Res.* 32:1792–1797. https://doi.org/10.1093/nar/gkh340